Agricultural and Forest Meteorology 373 (2025) 110768

Contents lists available at ScienceDirect

Agricultural and Forest Meteorology

journal homepage: www.elsevier.com/locate/agrformet

Weekly carbon and oxygen isotope dynamics in black spruce: A case study in the northeastern boreal forest of Quebec, Canada

Sepideh Namvar [a,*], Étienne Boucher [b], Annie Deslauriers [c], Fabio Gennaretti [d,e], Hubert Morin [c]

[a] Department of Biological Sciences and GEOTOP, Université du Québec à Montréal, 201, Président- Kennedy Ave, Montréal (QC) H2 × 3Y7, Canada
[b] Department of Geography, GEOTOP and Centre d'études nordiques, Université du Québec à Montréal, Montréal (QC) H2 × 3R9, Canada
[c] Departement des Sciences Fondamentales, Université du Québec à Chicoutimi, 555, boulevard de l'Université, Chicoutimi (QC) G7H 2B1, Canada
[d] Institut de Recherche sur les Forêts, Groupe de Recherche en Écologie de la MRC Abitibi, Université du Québec en Abitibi-Témiscamingue, 341, rue principale Nord, Amos (QC) J9T 2L8, Canada
[e] Department of Agricultural, Food and Environmental Sciences, Università Politecnica delle Marche, Piazza Roma, 22, 60121 Ancona, Italy

ARTICLE INFO

Keywords:
Dual-isotope approach
Carbon
Oxygen
Weekly monitoring
Tree ring
P_{ex} effect

ABSTRACT

The stable isotopic composition of carbon ($\delta^{13}C$) and oxygen ($\delta^{18}O$) in tree rings is widely used to explore tree eco-physiological dynamics across various time scales. However, interpreting these isotopic signals is challenging due to multiple interacting factors, including gas exchange at the leaf level, stored carbohydrate reserves, and xylem water, whose timing and interactions during the growing season remain poorly understood. In this study, weekly $\delta^{13}C$ and $\delta^{18}O$ signals were tracked within the cambial region and forming xylem of black spruce (*Picea mariana* (Mill.) BSP.) in boreal forests of Quebec, Canada. The study covered three consecutive growing seasons (2019–2021) at two forest sites with differing temperature and soil water content. Weekly isotopic profiles were developed for the cambial region ($\delta^{13}C_{cam}$ and $\delta^{18}O_{cam}$) and developing xylem cellulose ($\delta^{13}C_{xc}$ and $\delta^{18}O_{xc}$). Strong positive correlations were observed between $\delta^{13}C_{cam}$ and $\delta^{18}O_{cam}$, with an increasing trend along the growing season. Conversely, negative relationships were observed between $\delta^{13}C_{xc}$ and $\delta^{18}O_{xc}$, characterized by an increasing trend in $\delta^{13}C_{xc}$ and a decreasing trend in $\delta^{18}O_{xc}$. The results illustrated that stomatal conductance is the dominant physiological factor controlling seasonal fractionation of $\delta^{13}C_{cam}$ and $\delta^{18}O_{cam}$. Increasing proportional exchanges between xylem water and sugars at the sites of cellulose synthesis (i.e., P_{ex} effect) are thought to be strong enough to completely blur the observed trends in $\delta^{18}O_{cam}$ during the growing season. This suggests that $\delta^{18}O_{xc}$ signals differ from those originating in the earlier cambium sink. These findings highlight the need to carefully consider the processes influencing isotopic signals to avoid misinterpretations in dendroclimatological studies.

1. Introduction

Trees acclimate on daily to weekly time scales to ever-changing meteorological, environmental, and ecological conditions. To do this, they continuously adjust key processes like net photosynthesis (A_{net}) and stomatal conductance (g_s) to balance CO_2 uptake with H_2O losses while meeting sink demands (Flexas et al., 2013; Buckley 2017). These adjustments have critical impacts on gas and energy exchanges at the vegetation-atmosphere interface, ultimately providing important ecological services such as carbon sequestration and climate mitigation, for example through the regulation of transpiration rates (Beer et al. 2010). Despite considerable advances at the ecosystem level, derived from eddy-covariance data (Baldocchi 2020), the rate and synchronicity of A_{net} and g_s adjustments at the individual tree level remain poorly understood (Buckley 2017).

At the tree level, dendrochronological studies have predominantly utilized carbon and oxygen stable isotopes of tree ring to retrospectively document changes in A_{net} and g_s, linking these changes to shifting environmental conditions at the interannual scale (Raffalli-Delerce et al. 2004; Sass-Klaassen et al. 2005; Danis et al. 2006; Hilasvuori et al. 2009; Young et al. 2011; Szymczak et al. 2012; Naulier et al. 2014; Bégin et al. 2015). More specifically, the dual-isotope approach leverages the fact

* Corresponding author. Department of Biological Sciences, Université du Québec à Montréal, 201, Président-Kennedy Ave, Montréal (QC) H2 × 3Y7, Canada.
E-mail address: namvar.sepideh@courrier.uqam.ca (S. Namvar).

https://doi.org/10.1016/j.agrformet.2025.110768
Received 11 December 2024; Received in revised form 16 June 2025; Accepted 3 August 2025
Available online 8 August 2025

that carbon and oxygen stable isotopes are modified by gas exchanges at the leaf level, through processes such as A_{net} and g_s (Scheidegger et al. 2000; Grams et al. 2007). Therefore, tree ring stable isotope values provide valuable insights into metabolic adjustments under stress conditions. However, because measurements are made at the tree ring level, they yield only one isotopic value for an entire growing season, making it challenging to monitor adjustments on finer timescales (Rinne-Garmston et al. 2023). Moreover, this approach struggles to disentangle leaf-level physiological responses from other contributing factors (e.g., stored carbon reserves) that influence isotopic signals in tree rings.

Significant gaps persist in our mechanistic understanding of how physiological and climatic signals are transmitted into tree rings, particularly with regard to $\delta^{18}O$ (Martínez-Sancho et al. 2023). One of the main processes influencing the final $\delta^{18}O$ signature in tree rings is related to the synthesis of wood constituents in the xylem (Offermann et al. 2011; Treydte et al. 2014; Gessler et al. 2014). Proportional exchanges of oxygen occur with unenriched xylem (source) water during the conversion of sucrose to cellulose within the stem (Hill et al. 1995). This exchange of oxygen is known as "P_{ex} effect" and is largely influenced by biochemical cycling of hexose phosphates through intermediates such as UDP-glucose during cellulose synthesis. This process allows oxygen atoms, particularly those in carbonyl groups, to equilibrate with xylem water before incorporation into structural cellulose (Hill et al. 1995; Waterhouse et al. 2002). Consequently, a portion of carbonyl oxygen atoms (from enriched sugars) is exchanged with unenriched xylem water, thereby impairing the subsequent biochemical processes at the leaf level (Martínez-Sancho et al. 2023).

Previous studies proposed that P_{ex} represents a constant exchange rate during cellulose formation (Roden et al. 2000; Sternberg 2009). However, more recent research has shown that P_{ex} can vary from 0.29 to 0.77, depending on different factors such as species (Gessler et al. 2013) and environmental conditions (Luo and Sternberg 1992; Cernusak et al. 2005; Gessler et al. 2009; Song et al. 2014a; Belmecheri et al. 2018). Additionally, a recent study by Szejner et al. (2020) found that in two coniferous species, Pinus ponderosa (Douglas ex C. Lawson) and Pseudotsuga menziesii (Mirb.) Franco, P_{ex} increased across the tree ring. This increase was strongly associated with changes in wood anatomical features, particularly a reduction in lumen area as observed in latewood, suggesting a link between $\delta^{18}O$ exchange during cellulose synthesis and xylem structure in coniferous species.

Recent advances have enabled the generation of intra-annual isotope profiles through techniques such as sequential cutting of fully formed tree ring sections followed by IRMS analysis (Ogée et al. 2009; Pons and Helle 2011; Soudant et al., 2019; Fu et al. 2017; Belmecheri et al. 2018; Xu et al. 2022), or laser ablation methods (Schollaen et al. 2014; Loader et al. 2017; Saurer et al. 2023). Despite their important role in studying the isotopic composition of tree rings at intra-annual timescales, these methods encounter several challenges. Specifically, xylem cell formation is a predominantly successive developmental process (e.g., cell enlargement, cell wall thickening, etc.), with significant overlap in timing, rate, and duration (Fonti et al. 2018). This overlap restricts the ability of these sequential methods to detect short-term physiological and environmental impacts on carbon and oxygen isotope signals in tree rings. Furthermore, accurately identifying the source and timing of isotope fractionation at the leaf level and tracing the influence of previously synthesized carbohydrates (e.g., starch) on xylem development remain unclear (Rinne-Garmston et al. 2023). Additionally, estimating post-carboxylation processes introduces significant uncertainties (Gessler et al. 2014; Schiestl-Aalto et al. 2019).

To address these limitations and capture finer temporal dynamics, Namvar et al. (2024) developed a new method to monitor stable isotope fractionation in the growing cambium-xylem continuum as the tree ring forms. This method was initially applied to examine the dynamics of non-structural carbohydrates (NSCs) in the cambium and xylem of black spruce (Deslauriers et al. 2016), hybrid poplar (Deslauriers et al. 2009; Giovannelli et al. 2011) and Norway spruce (Simard et al. 2013). The findings confirmed that both the cambium and xylem derive carbohydrates from the same sources, most likely originating from the leaves throughout the growing season, with a minimal reliance on stored carbohydrates for stem growth (Deslauriers et al. 2016). Comparing these findings with oxygen isotope signals in the cambial region and developing xylem cellulose could provide new insights into the physiological processes driving seasonal carbon and oxygen stable isotope fractionation in the cambium-xylem continuum.

Here, we monitor weekly fluctuations of $\delta^{13}C$ and $\delta^{18}O$ within the cambial region ($\delta^{13}C_{cam}$ and $\delta^{18}O_{cam}$) and developing xylem cellulose ($\delta^{13}C_{xc}$ and $\delta^{18}O_{xc}$) of black spruce [*Picea mariana* (Mill.) BSP.] trees growing in two boreal forests of eastern Canada, using the method proposed by Namvar et al. (2024). Our analysis aims to provide insights into the dynamic shifts in $\delta^{13}C$ and $\delta^{18}O$ values within the vascular cambium-xylem continuum during the growing season in almost real time. We hypothesize that $\delta^{13}C$ and $\delta^{18}O$ values correlate within the cambial region and developing tree ring due to shared physiological constraints on carbon and oxygen fractionation originating at the leaf level. Indeed, both are expected to increase following the reduction in stomatal conductance during the growing season.

2. Materials and methods

2.1. Study sites

The study was conducted in mature black spruce stands located in the Saguenay-Lac-Saint-Jean area within the boreal forest of Quebec, Canada (Fig. 1). We used two particular sites: Simoncouche (SIM) and Bernatchez (BER), both featuring mature black spruce forests (Table 1). SIM is within the Simoncouche research station of the "Université du Québec a Chicoutimi" (48°13′ N, 71°15′ W, 338 m a.s.l.), situated in the Laurentide Wildlife Reserve. BER is at a higher elevation near Lake Poulin de Courval (48°51′ N, 70°20′ W, 611 m a.s.l.). Black spruce is the dominant species at both sites. The undergrowth is a typical mixed vegetation with various herbaceous and ericaceous shrub species (Dao et al. 2015). The region has a continental climate, marked by long cold winters and short warm summers (Balducci et al., 2021). Meteorological observations were available at each site using a tower equipped with an automatic data acquisition system and several measuring devices. These stations recorded various meteorological variables, including maximum temperature (T_{max}, °C), vapor pressure deficit (VPD, Kpa), photosynthetically active radiation (PAR, μmol/m^2/s), relative humidity (RH, %), precipitation (P, mm), and soil water content (VWC, m^3/m^3), on an hourly basis.

During the 2019–2021 study period, the mean annual air temperature in SIM was 3.2 °C, while BER experienced a lower mean of 0.6 °C (Table 1). During the growing season, specifically from May to October (2019–2021), mean temperatures were 12.8 °C in SIM and 10.3 °C in BER, indicating a colder and shorter growing season in BER. This is further reflected in the number of days with minimum daily temperatures above 5 °C, averaging 170±20 days in SIM and 139±15 days in BER (Rossi et al. 2011; Buttò et al. 2019). The two sites recorded similar mean precipitation levels during the growing season, with approximately 480 mm of rain each (average from May to October: 2019 to 2021). However, soil water content was higher at BER compared to SIM over the same period (average from May to October 2019–2021: BER, 0.34 m^3/m^3; SIM, 0.22 m^3/m^3) (Table 1). The difference in altitude, mean annual air temperature, and soil moisture (Table 1), between the two sites provided a framework to assess $\delta^{13}C$ and $\delta^{18}O$ dynamics under contrasting environmental conditions, thereby enriching the comparative dimension of this study.

2.2. Collection of cambial region and forming tree ring

Observations were conducted from late April to October in the years

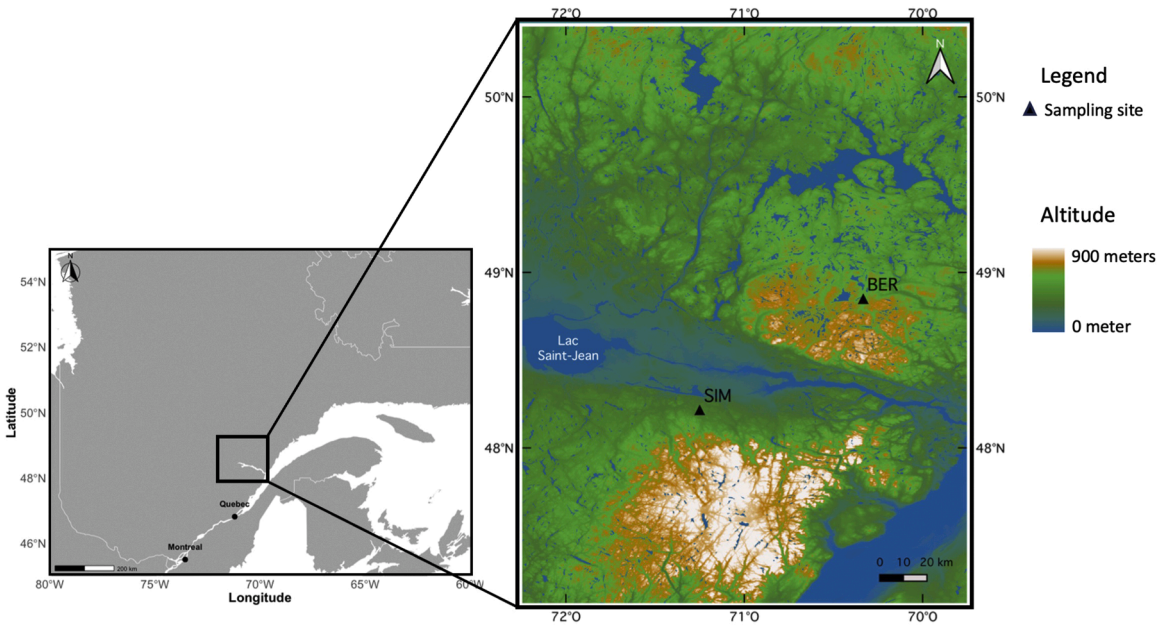

Fig. 1. Topography of the Saguenay-Lac-Saint-Jean region in Quebec, Canada, showing the locations of the two study sites: Simoncouche (SIM) and Bernatchez (BER). The map was designed in QGIS.

Table 1
Location, tree characteristics, and climatic conditions at the two study sites. Latitude (Lat.), longitude (Long.), altitude (Alt, meters above sea level). Annual and seasonal statistics for temperature (average), precipitation (sum), and soil water content (only seasonal, average) were calculated for the study years 2019-2021 at the two sites SIM and BER.

Code	Lat.	Long.	Alt (m a.s.l.)	May-Oct temperature (°C)	Annual temperature (°C)	May-Oct Precipitation (mm)	Annual Precipitation (mm)	May-Oct Soil water content (m^3/m^3)
SIM	48°13′	71°15′	338	12.8	3.2	484.3	640.6	0.22
BER	48°51′	70°20′	611	10.3	0.6	483	570.1	0.34

2019–2021 for SIM and 2020–2021 for BER. For each growing season, five mature black spruce trees with relatively similar stem diameters were selected at each site (Table S1). The selected trees were healthy, with over 50 % of branches alive in the crown. To avoid reaction wood, the tree samples were grown on flat surfaces with upright stems. From late April to October, we collected 13 to 22 rectangular strip samples, each measuring 3 × 6 cm, for each tree and study year using a chisel and rubber hammer (Table S2). The difference in sampling times (or number of samples) between the sites is attributed to variations in the length of the growing season. BER is located at a higher elevation and experiences cooler temperatures, which lead to a shorter growing season compared with SIM. As a result, fewer sampling times were possible at BER than at SIM. Moreover, BER is not accessible by road until the snow melts, which varies from year to year, further contributing to difference in the sampling period.

The strips, which included both bark and wood, were separated tangentially (Giovannelli et al. 2011), then frozen in liquid nitrogen and lyophilized at −50 °C for five days (Namvar et al. 2024). The cambial region, including some enlargement cells, was collected by scraping the inner bark and outermost xylem (Giovannelli et al. 2011). To reduce the costs of stable isotope analysis and ensure sufficient sample mass, cambial region material from all five trees was pooled for each sampling date. The samples were homogenized using a mixer mill (Retsch MM 400, Haan, Germany) at 30 Hz for 30 s. The forming tree ring was collected by cutting the transverse section under a binocular microscope with 10 × magnifying lenses and LED ring light. For narrower forming rings early in the growing season, the tangential area was scraped, the difference in color and brightness between the new cells and the previous year's ring facilitates scrapping the target cells (Namvar et al. 2024). Collected xylem samples were ground into fine particles for analysis, with pooling exclusively done for a few early-season samples lacking sufficient mass. Cellulose was extracted from xylem samples through a multi-step process to remove soluble organic compounds, lignin, and hemicellulose (Epstein et al. 1976). Samples placed in Teflon/polyester filter bags (ANKOM® XT4), were treated with a 1:1 solution of toluene and ethanol in an ultrasonic bath for 90 min, followed by an 80-minute treatment in acetone. The bags were then boiled for one hour to extract soluble organic compounds and subsequently bleached with sodium chlorite and acetic acid to remove lignin. Finally, pure α-cellulose was obtained by treating the samples with NaOH (17 % w/v) and acetic acid (10 %), followed by extensive rinsing and drying (Namvar et al. 2024).

2.3. Analysis of stable isotopes ratios

All isotopic measurements were conducted at the light-stable isotope geochemistry lab at the University of Quebec's Geotop facility in Montreal, Canada. For carbon isotope analysis, 0.5 to 0.8 mg of cellulose ($\delta^{13}C_{xc}$ for xylem samples) or pooled bulk material ($\delta^{13}C_{cam}$ for cambial samples) was weighed into tin capsules to ensure consistent CO_2 amounts across all samples and reference materials. These were analyzed using a Micromass Isoprime 100 isotope ratio mass spectrometer connected to an Elementar Vario MicroCube elemental analyzer in continuous flow mode, with an overall analytical uncertainty of ±0.1 ‰, excluding sample homogeneity and representativity. Two internal reference materials were used to normalize the results on the NBS19-LSVEC scale, and a third was analyzed as an unknown to assess the accuracy of the normalization. The total analytical uncertainty was

within ±0.1 ‰ (Hélie and Hillaire-Marcel 2021).

For oxygen isotope analysis, 0.3 mg of cellulose from xylem ($\delta^{18}O_{xc}$) and pooled cambial samples ($\delta^{18}O_{cam}$) was placed in silver cups to standardize mass amounts across samples. The analysis was performed using an Isoprime VisIon isotope ratio mass spectrometer coupled to an Elementar Vario PyroCube elemental analyzer in continuous flow mode. Results were normalized using two internal references on the VSMOW-SLAP scale, and a third reference was tested as an unknown to verify the accuracy of the process. The total analytical uncertainty was within ±0.3 ‰ (Hélie and Hillaire-Marcel 2021).

The weekly $\delta^{13}C$ and $\delta^{18}O$ profiles for the forming xylem cellulose were calculated by averaging the values from the five tree samples for each study year (Table S3 and S4). Inter-tree correlations for the $\delta^{13}C_{xc}$ series were previously analyzed by Namvar et al. (2024). The same analysis was performed here for $\delta^{18}O_{xc}$ profiles (Table S4, Figure S1). The differences in carbon and oxygen isotopic values between the cambial region and xylem cellulose (Table S3 and S4) likely reflect variations in the isotopic composition of the materials analyzed along the cambium-xylem continuum (see Namvar et al. 2024 for more details). The averaged $\delta^{13}C_{cam}$ and $\delta^{13}C_{xc}$ values were corrected to account for changes in atmospheric $\delta^{13}C$ ($\delta^{13}C_{atm}$) and Suess effect (Method S1). These corrected values are referred as $\delta^{13}C_{cam}$ and $\delta^{13}C_{xc}$ throughout the text.

2.4. Collection of rainwater

The rain samples were collected on a weekly basis, following the designated collection dates for the strips, during the growing seasons of 2020 and 2021 at both sites. To achieve this, a rain collector was mounted on the ground with no slope, ensuring that the funnel was approximately 30 cm above the ground to minimize wind turbulence (Figure S2a and b). The collector was positioned around 20 m away from the sampled trees in an open area. Each week, the collected rain samples were transferred into an accumulation bottle with a double cap, sealed with parafilm, and stored in the fridge for further analysis (Figure S2c).

To conduct the oxygen isotope analysis on rain samples, 1 ml of water was pipetted into a 2 ml vial and sealed with a septum cap. The samples were analyzed using a Picarro L2130-i Cavity Ring Down Spectroscopy (CRDS) system, with an overall analytical uncertainty of ±0.1 ‰. To ensure accuracy, three internal standards were used to adjust results to the VSMOW2-SLAP2 scale, and a fourth standard was tested as an unknown to verify the normalization accuracy. The reported standard deviations (1 sigma) reflect the variation among three replicate injections per sample.

2.5. Statistical analyses

Regression analysis was conducted to examine the seasonal trends of $\delta^{13}C$ and $\delta^{18}O$, as well as their significance, in both the cambial region and the developing tree ring (Table S5). The analysis of covariance (ANCOVA, VassarStats.net website, Vassar College Poughkeepsie, NY, USA) was used to compare the two regression lines of $\delta^{13}C$ and $\delta^{18}O$ in the cambial region and forming xylem cellulose across sites and study years. Pearson's correlations between the two chronologies ($\delta^{13}C$ and $\delta^{18}O$) were calculated to assess whether the profiles exhibited similar variations in the cambial region and developing xylem cellulose during the growing season as observed in other studies (McCarroll and Loader 2004; Ballantyne et al. 2010; Belmecheri and Lavergne 2020). This method was selected because the data met the key assumptions of normality and linearity. Normality was confirmed using the Shapiro-Wilk test (Table S6). To mitigate potential autocorrelation in the $\delta^{13}C$ and $\delta^{18}O$ time series, we performed an extra analysis by pre-whitening the data and fitting linear models as a function of the day of sampling (day of year; DOY). The obtained residuals of $\delta^{13}C$ and $\delta^{18}O$ were used for correlation analysis. This process removed time-dependent trends, allowing us to evaluate the correlation between $\delta^{13}C$ and $\delta^{18}O$ independently of temporal autocorrelation (Table S7).

Pearson's correlations were also employed to assess the relationships between $\delta^{13}C$, $\delta^{18}O$, and various meteorological parameters, as all series exhibited linear trends and met the assumption of linearity (Figure S3 and S4) and normality, as confirmed by Shapiro-Wilk test (Table S6). The same pre-whitening method was applied to the meteorological variables to perform correlations between the residuals of the isotopic data and the climate variables (Table S8 and S9). The weekly daytime (8h00 to 18h00) values of six different climate parameters: maximum temperature, vapour pressure deficit, photosynthetically active radiation, relative humidity, and soil volumetric water content, were averaged, and precipitation values were summed for the corresponding time periods (DOY) matching the sampling intervals for each year and site. Meteorological data were collected from on-site weather stations at each location.

To simulate the seasonal dynamics of the fraction of oxygen atoms exchanged with xylem water, known as P_{ex} effect, P_{ex} was modeled under three scenarios: a constant value of 0.4, a linear increasing P_{ex} from 0.3 to 0.5, and a linear decrease from 0.5 to 0.3 (Szejner et al. 2020). To represent seasonal variation, P_{ex} was modeled as a linear function of the day of year (DOY), starting from an initial value $\left(P_{ex}^{start}\right)$ at the beginning of the growing season and changing gradually to a final value $\left(P_{ex}^{end}\right)$ by the end of the season. The rate of change in P_{ex} (Slope, rate per day) was calculated from the beginning (DOY_{start}) to the end of the growing season (DOY_{end}), using the following equation:

$$\text{Slope} = \frac{P_{ex}^{end} - P_{ex}^{start}}{DOY_{end} - DOY_{start}} \quad (1)$$

The P_{ex} values were then generated to increase or decrease linearly over the DOY range, either from 0.3 to 0.5 (increasing trend) or from 0.5 to 0.3 (decreasing trend) as follows:

$$P_{ex(date=n)} = P_{ex}^{start} + Slope\ (DOY_{(date=n)} - DOY_{start}) \quad (2)$$

To test the effect of P_{ex} on $\delta^{18}O_{xc}$ signals during the growing season, a model was developed to simulate $\delta^{18}O_{xc}$ ($\delta^{18}O_{xc\text{-}sim}$), using the following equation (Szejner et al. 2020):

$$\delta 18O_{xc-sim\ (date=n)} = P_{ex(date=n)}\ (\ \delta 18O_{xw\ (date=n)} + \varepsilon c) + (1 - P_{ex(date=n)})(\delta 18O_{lw(date=n)} + \varepsilon c) \quad (3)$$

Where ε_c represents the average biochemical fractionation between water and organic materials, which was set to a constant value of 27 ‰. The isotopic composition of source water, $\delta^{18}O_{xw}$, was represented by $\delta^{18}O_{rain}$ values. $\delta^{18}O_{lw}$ refers to the isotopic composition of water at the leaf evaporation sites, here approximated by $\delta^{18}O_{cam}$. The P_{ex} values were obtained from Eq. (2) for linear variability or assumed constant during the growing season (P_{ex}=0.4). To evaluate the influence of P_{ex} on $\delta^{18}O_{xc\text{-}sim}$, regression analyses (ANCOVA) were performed using standardized $\delta^{18}O_{cam}$ and $\delta^{18}O_{xc\text{-}sim}$ series. The resulting regression slopes were then compared across different sites and years to determine which P_{ex} scenario best reflects the observed $\delta^{18}O_{xc}$ patterns.

3. Results

3.1. Seasonal trends in $\delta^{13}C$ and $\delta^{18}O$ in the cambial region and developing tree ring

During the full growing season, both $\delta^{13}C_{cam}$ and $\delta^{18}O_{cam}$ profiles showed increasing trends with varying significance levels across almost all study years, except in SIM 2021 where $\delta^{13}C_{cam}$ and $\delta^{18}O_{cam}$ profiles showed downward trends (β=−0.003, $p < 0.01$; β=−0.002, $p > 0.1$, respectively) (Fig. 2, Table S5). An insignificant decreasing trend was also observed in BER 2021 $\delta^{13}C_{cam}$ series (β=−0.002, $p > 0.1$). The $\delta^{13}C_{cam}$ increasing series were significant in SIM 2019 (β=+0.006, $p < 0.001$) and BER 2020 (β=+0.005, $p < 0.001$), while the $\delta^{18}O_{cam}$ rising

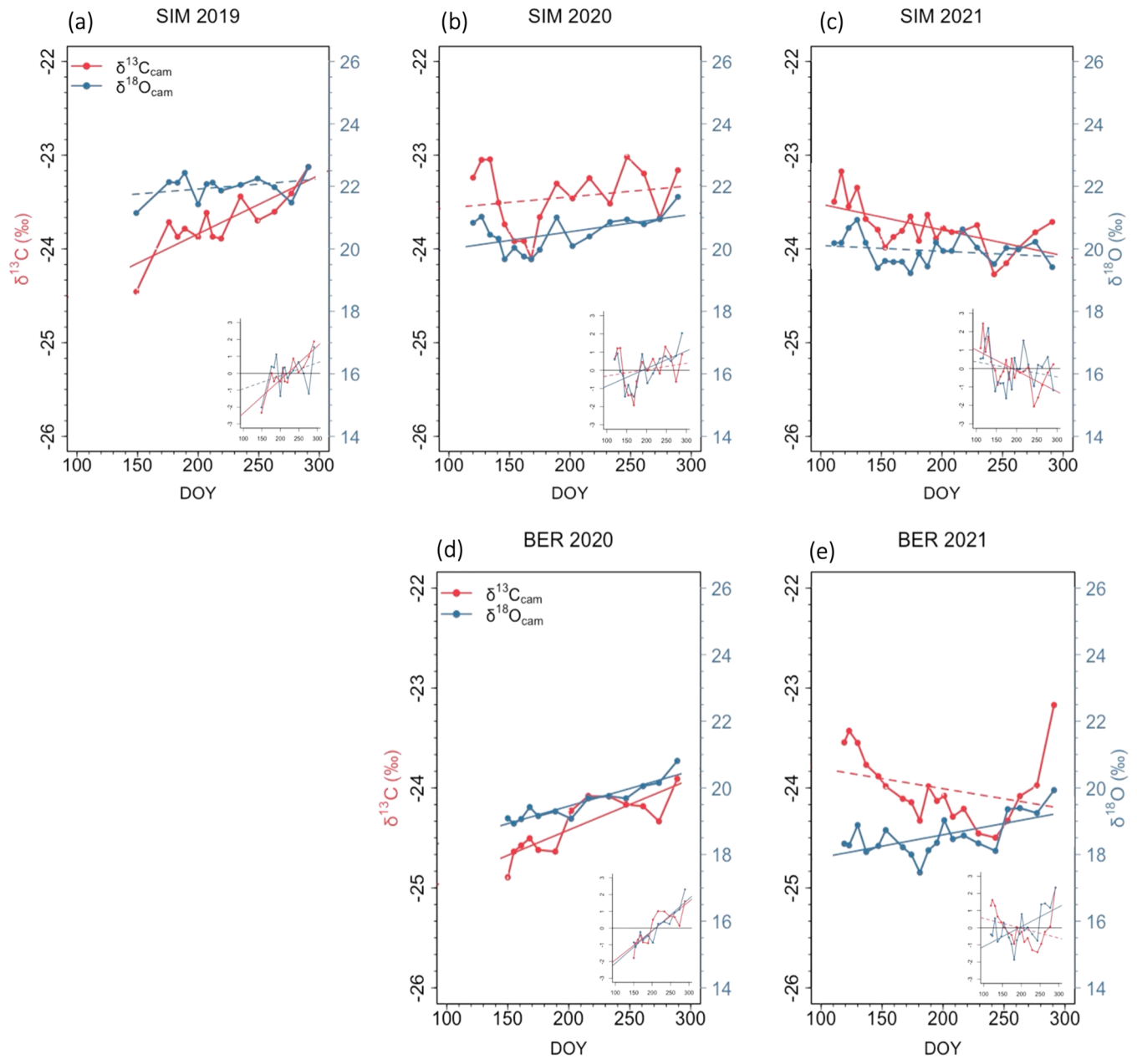

Fig. 2. Intra-annual $\delta^{13}C_{cam}$ and $\delta^{18}O_{cam}$ profiles in SIM (a, b, c) and BER (d, e). The red lines represent the $\delta^{13}C_{cam}$ values for the full growing season in each study year. The blue lines represent $\delta^{18}O_{cam}$ values for the same period during the growing season. Solid lines denote regression lines with significant slopes, and dashed lines indicate insignificant slopes. The insets represent standardized $\delta^{13}C_{cam}$ and $\delta^{18}O_{cam}$ profiles (*z*-scores) in each site and study year (see Figure S5 for more details).

patterns were significant in SIM 2020 (β=+0.006, $p < 0.05$), BER 2020 (β=+0.011, $p < 0.001$) and BER 2021 (β=+0.007, $p < 0.01$) (Table S5). In SIM, slopes in $\delta^{13}C_{cam}$ were similar to those of $\delta^{18}O_{cam}$ across three years of 2019 ($F = 0.9$, $p = 0.4$), 2020 ($F = 2.5$, $p = 0.1$), and 2021 ($F = 0.1$, $p = 0.7$), although with different intercepts (2019: $F = 140{,}730.7$, $p < 0.0001$; 2020: $F = 87{,}473.4$, $p < 0.0001$; 2021: $F = 174{,}720.8$, $p < 0.0001$). However, in BER, significant differences were observed between $\delta^{13}C_{cam}$ and $\delta^{18}O_{cam}$ profiles both in terms of slopes (2020: $F = 12.0$, $p < 0.01$; 2021: $F = 11.4$, $p < 0.01$) and intercepts (2020: $F = 233{,}382.2$, $p < 0.0001$; 2021: $F = 81{,}335$, $p < 0.0001$).

From the perspective of intra-annual variability, consistent and significant intra-annual covariations between $\delta^{13}C_{cam}$ and $\delta^{18}O_{cam}$ profiles were observed at both sites and during all study years (Table 2, Fig. 2). In SIM, positive correlations were evident between the two series during study years of 2019 (r=+0.58, $p < 0.05$), 2020 (r=+0.73, $p < 0.001$) and 2021 (r=+0.38, $p < 0.1$). Similarly, in BER, positive relationships were observed for the years 2020 (r=+0.76, $p < 0.01$) and 2021 (r=+0.35, $p > 0.1$). The strong positive relationships remained between the pre-whitened detrended residuals of $\delta^{13}C_{cam}$ and $\delta^{18}O_{cam}$ series in SIM

Table 2
Correlation coefficients and ρ values between $\delta^{13}C$ and $\delta^{18}O$ values in the cambium and xylem cellulose in different study sites and years.

Pearson's correlation	SIM 2019	SIM 2020	SIM 2021	BER 2020	BER 2021
Between $\delta^{13}C_{cam}$ and $\delta^{18}O_{cam}$	0.58 ($\rho<0.05$)	0.73 ($\rho<0.001$)	0.38 ($\rho<0.1$)	0.76 ($\rho<0.01$)	0.35 ($\rho>0.1$)
Between $\delta^{13}C_{xc}$ and $\delta^{18}O_{xc}$	−0.60 ($\rho<0.1$)	−0.36 ($\rho>0.1$)	−0.07 ($\rho>0.1$)	−0.45 ($\rho>0.1$)	−0.26 ($\rho>0.1$)

2019 (r=+0.60, $p < 0.05$), SIM 2020 (r=+0.76, $p < 0.01$), and BER 2021 (r=+0.70, $p < 0.01$) (Table S7).

In contrast to the stable isotope profiles in the cambial region, $\delta^{13}C_{xc}$ and $\delta^{18}O_{xc}$ series in the developing tree rings displayed opposite seasonal trends (Table S5, Fig. 3). Specifically, $\delta^{13}C_{xc}$ series showed significant increasing trends both in SIM (2019: β=+0.008, $p < 0.01$; 2020: β=+0.004, $p < 0.1$), and BER (2020: β=+0.005, $p < 0.1$; 2021: β=+0.006, $p < 0.01$). In contrast, $\delta^{18}O_{xc}$ series exhibited decreasing trends at both study sites, while significant only in SIM 2019 (β=−0.019, $p < 0.01$), and BER 2020 (β=−0.008, $p < 0.05$) (Table S5). We observed significant differences between the regression slopes of $\delta^{13}C_{xc}$ and $\delta^{18}O_{xc}$ series both in SIM (2019: $F = 38.3$, $p < 0.001$; 2020: $F = 15.1$, $p < 0.01$) and BER (2020: $F = 12.9$, $p < 0.01$; 2021: $F = 10.8$, $p < 0.01$) (Fig. 3).

Concerning intra-annual variability, $\delta^{13}C_{xc}$ and $\delta^{18}O_{xc}$ showed negative correlations across the three study years in SIM 2019 (r=−0.60, $p < 0.1$), 2020 (r=−0.36, $p > 0.1$) and 2021 (r=−0.07, $p > 0.1$), as well as in BER 2020 (r=−0.45, $p > 0.1$) and BER 2021 (r=−0.26, $p > 0.1$) (Table 2). The pre-whitened detrended residuals of $\delta^{13}C_{xc}$ and $\delta^{18}O_{xc}$ exhibited insignificant positive correlations in SIM during 2019 (r=+0.26, $p > 0.1$), 2020 (r=+0.24, $p > 0.1$), and 2021 (r=+0.02, $p > 0.1$), while weak negative correlations were observed in BER for 2020 and 2021 (r=−0.01, $p > 0.1$; r=−0.25, $p > 0.1$ respectively) (Table S7).

3.2. Relationships between $\delta^{18}O$ and $\delta^{18}O_{rain}$ series

Significant negative relationships were observed between $\delta^{18}O_{cam}$ and $\delta^{18}O_{rain}$ (r =−0.45, $p < 0.1$) and $\delta^{18}O_{xc}$ and $\delta^{18}O_{rain}$ (r =−0.53, $p < 0.05$) in SIM 2021. All other relationships between $\delta^{18}O$ in the cambium or xylem and $\delta^{18}O_{rain}$ were non-significant in both sites and study years (Fig. 4, Table 3).

3.3. Relationships between $\delta^{13}C$ and $\delta^{18}O$ series and climate data

Negative correlations were identified when comparing $\delta^{13}C_{cam}$ and $\delta^{18}O_{cam}$ series with meteorological variables of T_{max}, VPD, and PAR, across almost all study years, though they were only significant in certain cases (Table 4). Conversely, positive links were detected between $\delta^{13}C_{cam}$ and $\delta^{18}O_{cam}$ profiles and RH both in SIM and BER, with significant values in a few series in both sites (Table 4). In both sites and most

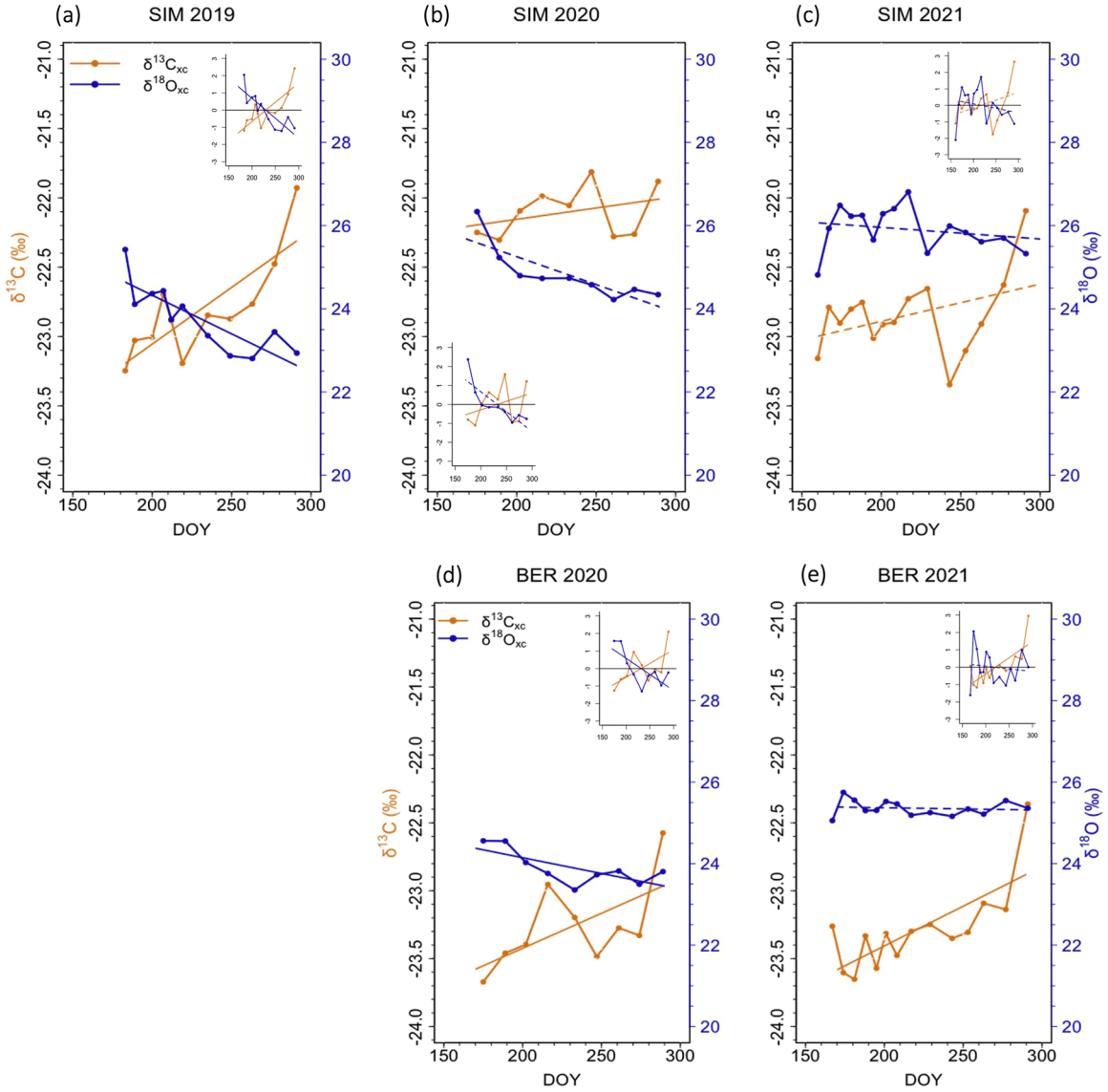

Fig. 3. Intra-annual $\delta^{13}C_{xc}$ and $\delta^{18}O_{xc}$ profiles in SIM (a, b, c) and BER (d, e). The orange lines represent the $\delta^{13}C_{xc}$ values over the growing season in each study year. The blue lines represent $\delta^{18}O_{xc}$ values for the same period during the growing season. Solid lines denote regression lines with significant slopes, and dashed lines indicate insignificant slopes. The insets represent standardized $\delta^{13}C_{xc}$ and $\delta^{18}O_{xc}$ profiles (z-scores) in each site and study year (see Figure S6 for more details).

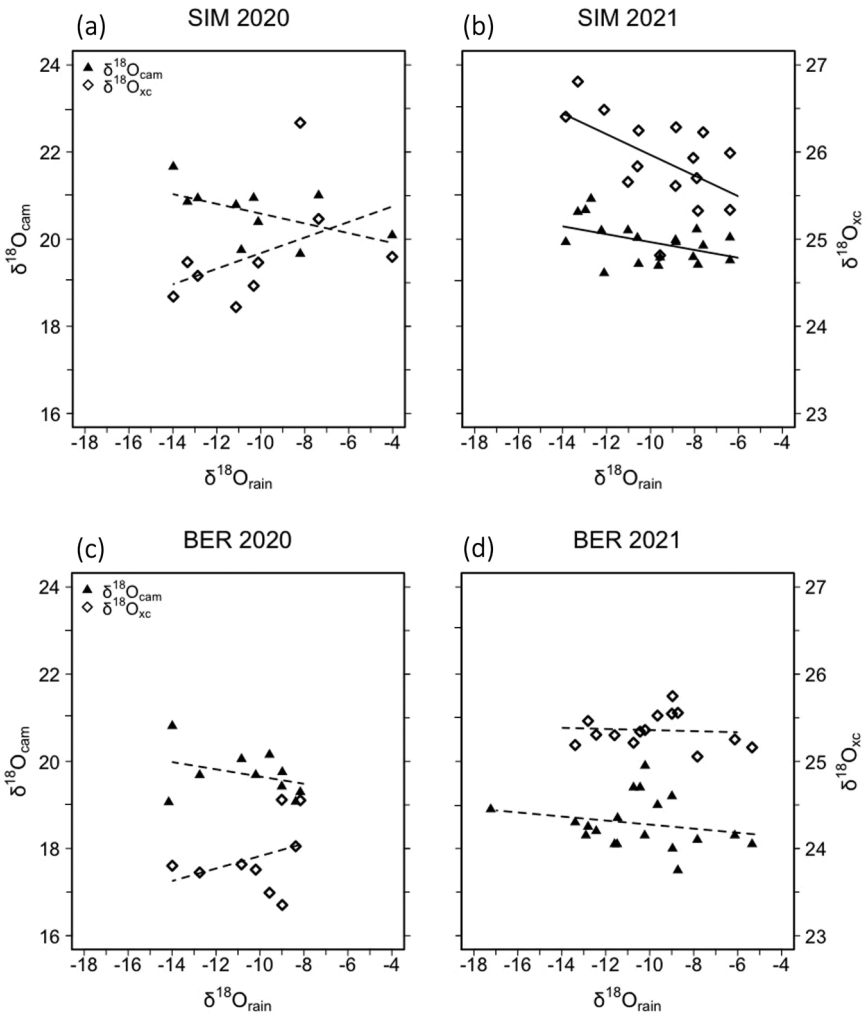

Fig. 4. Scatterplots and regression lines of weekly $\delta^{18}O_{cam}$ and $\delta^{18}O_{xc}$ as a function of $\delta^{18}O_{rain}$ in SIM 2020 (a), SIM 2021 (b), and BER 2020 (c) and BER 2021 (d). Solid lines denote regression lines with significant slopes, and dashed lines indicate insignificant slopes.

Table 3
Correlation coefficients for the relationships between $\delta^{18}O_{cam}$ or $\delta^{18}O_{xc}$ values and $\delta^{18}O_{rain}$ in different study sites and years.

Pearson's correlation	SIM 2020	SIM 2021	BER 2020	BER 2021
Between $\delta^{18}O_{cam}$ and $\delta^{18}O_{rain}$	−0.54 (ρ>0.1)	−0.45 (ρ<0.1)	−0.35 (ρ>0.1)	−0.21 (ρ>0.1)
Between $\delta^{18}O_{xc}$ and $\delta^{18}O_{rain}$	0.45 (ρ>0.1)	−0.53 (ρ<0.05)	0.34 (ρ>0.1)	−0.08 (ρ>0.1)

study years, no significant relationships were found between the sum of daytime P and mean daytime VWC and either $\delta^{13}C_{cam}$ or $\delta^{18}O_{cam}$ profiles, except in SIM 2019, where strong positive interactions were observed between P and $\delta^{13}C_{cam}$ (r=+0.84, p < 0.01). Similar positive links were found between VWC and $\delta^{13}C_{cam}$ in SIM 2021 (r=+0.59, p < 0.05), $\delta^{18}O_{cam}$ in SIM 2020 (r=+0.71, p < 0.05) and $\delta^{18}O_{cam}$ in BER 2020 (r=+0.68, p < 0.05) (Table 4). In terms of pre-whitened detrended residuals, significant relationships between $\delta^{13}C_{cam}$ or $\delta^{18}O_{cam}$ and meteorological variables varied across sites and years (Table S8). T_{max}, VPD, and PAR were particularly influential in 2020 and 2021, showing strong negative correlations with both $\delta^{13}C_{cam}$ and $\delta^{18}O_{cam}$ in both sites. In contrast, RH, P and VWC had more sporadic, site-specific effects,

Table 4
Correlation coefficients for the relationships between $\delta^{13}C_{cam}$ or $\delta^{18}O_{cam}$ values and different weekly meteorological variables of daytime averages (8h00 to 18h00) over the growing season. maximum temperature (T_{max}), vapour pressure deficit (VPD), photosynthetically active radiation (PAR), relative humidity (RH), precipitation (P), soil volumetric water content (VWC), (* ρ < 0.1, ** ρ < 0.05, *** ρ < 0.01).

Site/year	SIM 2019		SIM 2020		SIM 2021		BER 2020		BER 2021	
	$\delta^{13}C_{cam}$	$\delta^{18}O_{cam}$	$\delta^{13}C_{cam}$	$\delta^{18}O_{cam}$	$\delta^{13}C_{cam}$	$\delta^{18}O_{cam}$	$\delta^{13}C_{cam}$	$\delta^{18}O_{cam}$	$\delta^{13}C_{cam}$	$\delta^{18}O_{cam}$
T_{max}	−0.49	−0.12	−0.33	−0.68**	−0.13	−0.05	−0.62*	−0.92***	−0.59**	−0.64**
VPD	−0.61*	−0.14	−0.49	−0.67**	0.01	−0.11	−0.71**	−0.77**	−0.45	−0.59**
PAR	−0.79***	−0.24	−0.56*	−0.81***	0.27	−0.10	−0.65*	−0.92***	−0.42	−0.64**
RH	0.73**	0.18	0.71**	0.69**	−0.10	0.21	0.81**	0.72**	0.34	0.49*
P	0.84***	0.48	0.16	−0.23	0.03	−0.06	0.54	0.07	−0.21	−0.46
VWC	−0.31	0.23	0.30	0.71**	0.59**	−0.30	0.29	0.68**	0.07	−0.45

indicating a less consistent influence (Table S8).

$\delta^{13}C_{xc}$ and $\delta^{18}O_{xc}$ profiles exhibited divergent associations with various meteorological variables (Table 5). Negative relationships were consistently noted between $\delta^{13}C_{xc}$ and T_{max}, VPD, and PAR across all study years, though they were only significant in certain cases. In contrast, positive correlations were observed between T_{max}, VPD, and PAR and $\delta^{18}O_{xc}$ in SIM 2019, SIM 2020, and BER 2020. Strong negative relationships were detected between $\delta^{18}O_{xc}$ and RH in SIM 2019 (r=−0.64, $p < 0.05$), and BER 2020 (r=−0.66, $p < 0.1$). In SIM 2019, significant positive relationships were evident between $\delta^{18}O_{xc}$ and VWC (r=+0.72, $p < 0.05$) (Table 5). Additionally, the pre-whitened detrended residuals of $\delta^{13}C_{xc}$ or $\delta^{18}O_{xc}$ exhibited variable responses to meteorological factors (Table S9), with VWC and RH generally showing more consistent positive effects, while T_{max} and VPD played a more site- and year-specific role in shaping the isotopic dynamics of the developing xylem (Table S9).

3.4. Comparison between $\delta^{18}O_{cam}$, $\delta^{18}O_{xc}$, and $\delta^{18}O_{xc\text{-}sim}$ across p_{ex} scenarios

In the decreasing P_{ex} scenario, the slopes of $\delta^{18}O_{xc\text{-}sim}$ were similar to those of observed $\delta^{18}O_{cam}$ across SIM 2020 (ANCOVA test between standardized values, $F = 0.2$, $p = 0.7$), BER 2020 ($F = 0.3$, $p = 0.6$), and BER 2021 ($F = 0.5$, $p = 0.5$) (Fig. 5a, 5c, and 5d respectively). The only exception was SIM 2021, where a significant difference was found between the two slopes ($F = 6.02$, $p < 0.05$) (Fig. 5b). Similarly, the constant P_{ex} scenario had little influence on the $\delta^{18}O_{cam}$ slope in 2021, with no significant differences observed in SIM ($F = 0.2$, $p > 0.1$) and BER ($F = 0.9$, $p > 0.1$). However, in 2020, the effect was more pronounced, as significant differences were detected in both SIM ($F = 12.6$, $p < 0.01$) and BER ($F = 13.4$, $p < 0.01$) (Fig. 5).

The increasing P_{ex} scenario induced a clear shift on the slope of $\delta^{18}O_{cam}$ (Fig. 5). It transformed the observed increasing $\delta^{18}O_{cam}$ slope into a decreasing trend in $\delta^{18}O_{xc\text{-}sim}$, consistent with the pattern observed in measured $\delta^{18}O_{xc}$ (i.e., decreasing trends $\delta^{18}O_{xc}$). Under this condition, significant differences emerged between the $\delta^{18}O_{cam}$ and $\delta^{18}O_{xc\text{-}sim}$ slopes in both SIM (2020: $F = 42.5$, $p < 0.01$; 2021: $F = 13.1$, $p < 0.01$) and BER (2020: $F = 83.6$, $p < 0.01$; 2021: $F = 64.3$, $p < 0.01$) (Fig. 5). In contrast, comparison between the slopes of $\delta^{18}O_{xc}$ and $\delta^{18}O_{xc\_sim}$ under increasing P_{ex} (from 0.3 to 0.5) revealed no significant differences in SIM 2020 ($F = 0.4$, $p > 0.1$), SIM 2021 ($F = 1.6$, $p > 0.1$), and BER 2020 ($F = 0.8$, $p > 0.1$) (Fig. 5a, 5b, 5c respectively), except for BER 2021 ($F = 3.1$, $p = 0.09$) (Fig. 5d).

4. Discussion

This study represents the first attempt to monitor weekly variations in carbon and oxygen stable isotopes within the cambial region ($\delta^{13}C_{cam}$ and $\delta^{18}O_{cam}$) and developing xylem cellulose ($\delta^{13}C_{xc}$ and $\delta^{18}O_{xc}$) in black spruce trees. These data allowed us to distinguish between the processes driving isotope variation in the cambial region and those affecting developing xylem cellulose. Our findings underscore the importance of accounting for these processes to avoid misinterpretation of isotopic signals in dendroclimatological studies.

Our initial hypothesis proposed that $\delta^{13}C$ and $\delta^{18}O$ values in the cambial region would correlate due to shared physiological constraints on stable isotopes fractionation originating at the leaf level. The results of this study confirm this hypothesis and suggest that stomatal conductance (g_s) regulation in the needles of black spruce is likely the dominant factor controlling the seasonal fractionation of $\delta^{13}C_{cam}$ and $\delta^{18}O_{cam}$ in our study region. Both $\delta^{13}C_{cam}$ and $\delta^{18}O_{cam}$ series exhibited consistent seasonal enrichment patterns during the growing season in nearly all study years and sites (Fig. 2), with no strong relationships observed between $\delta^{18}O_{rain}$ and $\delta^{18}O_{cam}$ (Table 3). This pattern aligns with the dual-isotope theory (Scheidegger et al. 2000; Siegwolf et al. 2023), which attributes such enrichment to the concurrent influence of g_s on the fractionation of both isotopes. Indeed, the observed enrichment cannot be explained by changes in photosynthesis, as photosynthesis declines toward the end of the growing season. A previous study on European beech (*Fagus sylvatica* L.) reported similar findings, showing strong positive correlations between $\delta^{13}C$ and $\delta^{18}O$ in the organic matter of phloem sap, further underscoring the dominant influence of g_s on both carbon and oxygen isotopic signals (Keitel et al. 2003). Furthermore, if $\delta^{13}C_{cam}$ variations were driven by changes in A_{net}, $\delta^{18}O_{cam}$ series would diverge from those of $\delta^{13}C_{cam}$. This was not the case here, as we observed strong positive correlations between $\delta^{13}C_{cam}$ and $\delta^{18}O_{cam}$ profiles in almost all study years (Table 2), a pattern related to stomatal regulation and not photosynthetic control of $\delta^{13}C_{cam}$ (Farquhar et al. 1998; Scheidegger et al. 2000). However, SIM 2021 appears to be an exception. In this year, both $\delta^{13}C_{cam}$ and $\delta^{18}O_{cam}$ showed trends distinct from those observed in other years (Fig. 2c), and a significant correlation between $\delta^{18}O_{cam}$ and $\delta^{18}O_{rain}$ was detected (Table 3). This suggests that source water may play a larger role in influencing $\delta^{18}O_{cam}$ values in SIM 2021. This anomaly indicates that the dual-isotope approach may not reliably capture stomatal conductance limitations in all years, particularly when external environmental conditions, such as changes in source water composition, exert a stronger influence.

The dual isotope theory primarily addresses leaf-level fractionations, but it can be applied to carbon and oxygen in other tissues, provided that post-carboxylation processes are minimal (Gessler et al. 2009; Siegwolf et al. 2021; Siegwolf et al. 2023). The strong similarity observed in $\delta^{13}C_{cam}$ and $\delta^{18}O_{cam}$ variations in this study further supports the notion that post-carboxylation processes played a minor role, if any, in the overall fractionation of carbon isotopes, up to its fixation in tree-ring cellulose (Barbour et al. 2002; Klein et al. 2005; Gessler et al. 2009). If such processes were to dominate, notable differences between $\delta^{13}C_{cam}$ and $\delta^{18}O_{cam}$ would arise, both in terms of their trends and inter-weekly variability. This is because only carbon isotopes are affected by post-carboxylation processes, while the $\delta^{18}O$ signature of NSCs is unlikely to be altered during phloem transport of assimilates to the cambial region (Roden et al. 2000; Gessler et al. 2009; Siegwolf et al. 2023). Indeed, sucrose which is the main sugar exported from the leaves, carries no free carbonyl group that could exchange oxygen atoms with water during its movement from the leaves to the cambial region (Gessler et al. 2014). These findings are in conformity with a study by Gessler et al. (2009), who found rather consistent transfer of $\delta^{13}C$ and

Table 5
Correlation coefficients for the relationships between $\delta^{13}C_{xc}$ or$\delta^{18}O_{xc}$ values and different weekly meteorological variables of daytime averages (8h00 to 18h00) over the growing season. maximum temperature (T_{max}), vapour pressure deficit (VPD), photosynthetically active radiation (PAR), relative humidity (RH), precipitation (P), soil volumetric water content (VWC), (* $\rho < 0.1$, ** $\rho < 0.05$, *** $\rho < 0.01$).

Site/year	SIM 2019		SIM 2020		SIM 2021		BER 2020		BER 2021	
	$\delta^{13}C_{xc}$	$\delta^{18}O_{xc}$	$\delta^{13}C_{xc}$	$\delta^{18}O_{xc}$	$\delta^{13}C_{xc}$	$\delta^{18}O_{xc}$	$\delta^{13}C_{xc}$	$\delta^{18}O_{xc}$	$\delta^{13}C_{xc}$	$\delta^{18}O_{xc}$
T_{max}	−0.51	0.22	−0.18	0.57*	−0.48*	−0.02	−0.64*	0.51	−0.54**	−0.11
VPD	−0.58*	0.51	−0.34	0.55	−0.48*	−0.17	−0.66*	0.67*	−0.51*	−0.24
PAR	−0.71**	0.67**	−0.48	0.24	−0.44	0.13	−0.71**	0.56	−0.63**	−0.17
RH	0.69**	−0.64**	0.63*	−0.25	0.46*	0.09	0.76**	−0.66*	0.45	0.36
P	0.85***	−0.47	0.10	−0.29	0.12	0.16	0.42	−0.46	−0.37	0.37

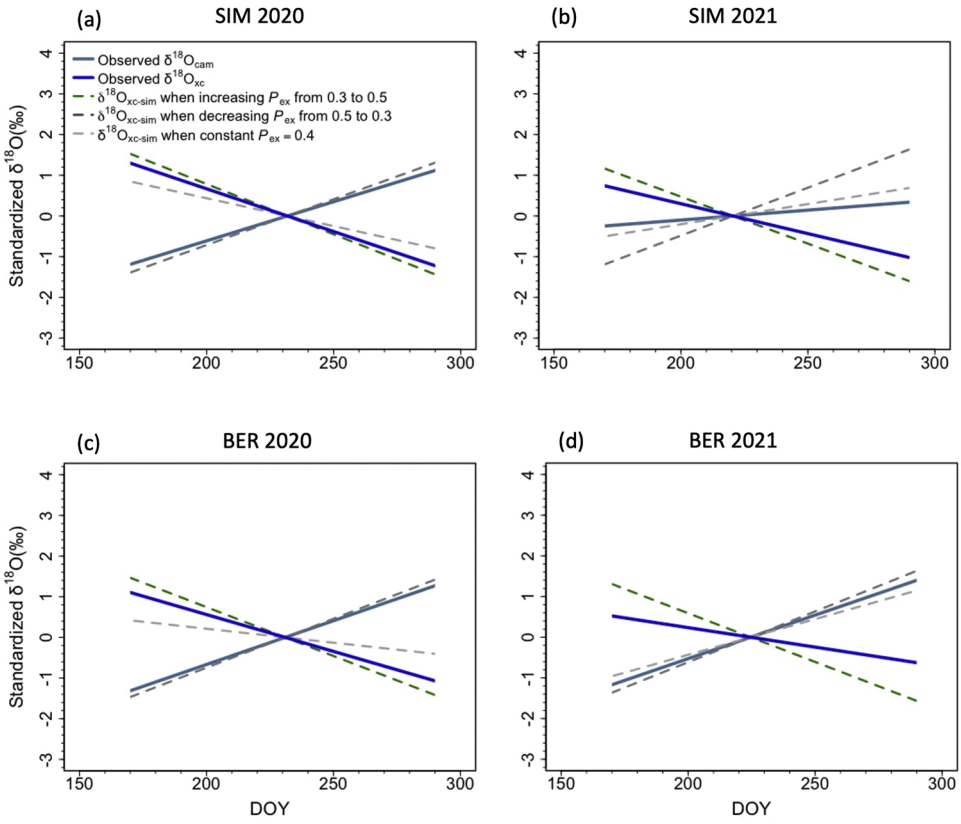

Fig. 5. Comparison of the slopes between observed $\delta^{18}O_{cam}$, $\delta^{18}O_{xc}$, and simulated $\delta^{18}O_{xc}$ ($\delta^{18}O_{xc\text{-}sim}$) under three P_{ex} scenarios during the growing season: increasing P_{ex} (from 0.3 to 0.5), decreasing P_{ex} (from 0.5 to 0.3), and constant P_{ex} (0.4), across different sites and study years.

$\delta^{18}O$ signals from canopy to the trunk phloem and cellulose or wood in *P. sylvestris*, during the entire growing season. In addition, previous studies indicate that the $\delta^{18}O$ in leaf water is reflected in the oxygen isotope signature of compounds synthesized in the leaves and potentially transported in the phloem (Roden and Ehleringer 1999; Barbour et al. 2000), suggesting minimal changes in $\delta^{18}O$ in phloem sap during transport through the tree trunk.

The neglectable effect of post-carboxylation processes, combined with a strong correlation between $\delta^{13}C_{cam}$ and $\delta^{13}C_{xc}$ as evidenced by Namvar et al. (2024), finally supports the fact that both cambium and xylem cells derive carbohydrates from a similar source during the growing season. Indeed, NSCs most likely derive from recently-produced photo assimilates incoming from the leaves, with minimal contribution from stored NSCs, mostly in the form of ^{13}C-enriched starch, for growth purposes in our spruce species (Simard et al. 2013; Gessler et al. 2014; Deslauriers et al. 2016). This aligns with the recent findings of Rinne--Garmston et al. (2023), who observed that intra-seasonal dynamics of $\delta^{13}C$ in primary photosynthates were clearly reflected in the tree ring $\delta^{13}C$ signals of 7-year-old *Pinus sylvestris*, suggesting a negligible impact of reserve use on tree ring $\delta^{13}C$ values. Additionally, lower variations in ^{13}C-enriched starch were observed in the cambium of larch and spruce trees during the growing season. This suggests that a constant supply of fresh assimilates to the cambium-xylem continuum may be the dominant process feeding secondary growth in our spruce trees (Simard et al. 2013; Rinne et al. 2015).

Increasing $\delta^{13}C_{cam}$ and $\delta^{18}O_{cam}$ trends do not exclusively originate from changing meteorological conditions, during the growing season (Table 4). Indeed, most studies in dendroclimatology indicate that increasing moisture stress towards the end of the growing season may lead to elevated $\delta^{13}C$ values in tree rings (Sarris et al. 2013; Castagneri et al. 2018; Xu et al. 2022). For instance, reduced precipitation and soil water content, excessively high temperatures and a lower relative humidity may all contribute to the limitation of g_s in the needles of evergreen conifers. In turn, this could lead to increasing $\delta^{13}C$ and $\delta^{18}O$ trends in different tissues of trees. Conversely, in our study region, growing seasons become increasingly cold and wet towards their end. Such conditions are unlikely to trigger a typical water-stress-induced g_s reduction, which would increase $\delta^{13}C_{cam}$ and $\delta^{18}O_{cam}$ (Namvar et al. 2024).

In the absence of climate conditions conductive to a moisture stress response of g_s, three alternative causes are proposed that individually or jointly explain the observed cumulative increasing trends in $\delta^{13}C_{cam}$ and $\delta^{13}O_{cam}$ in almost all study year and sites (Fig. 2). First, reduced light intensity (PAR) and temperature (T_{max}) toward the end of the growing season may lead to a gradual decline in net photosynthesis (A_{net}), which in turn may force a greater reduction in g_s resulting in increasing $\delta^{13}C_{cam}$ values (Farquhar and Sharkey 1982; Siegwolf et al. 2023). Additionally, increasingly limited light conditions may lead to higher $\delta^{18}O$ values in leaf water due to lower transpiration rates. This effect is further compounded by a progressive decline in black spruce water content and reduced turnover of leaf water from soil water toward the end of the growing season (Péclet effect; Farquhar and Lloyd 1993, Barbour and Farquhar 2000, Turcotte et al. 2011). Indeed, black spruce trees gradually dehydrate their stem tissues in response to decreasing autumn temperatures, leading to maximum stem shrinkage in winter (Turcotte et al. 2009). The second alternative involves mechanisms of preparation for overwintering to minimize potential damage to tree hydraulic functions and living cells (Burke et al. 1976; Charrier et al. 2013; Arora 2018). To mitigate such damage, trees reduce water content and enhance residual evaporation through their needles (g_{min}) to prevent ice crystal formation in living cells (Bozonnet et al. 2024; Charrier and Améglio 2024). Reduced water uptake in early autumn also leads to less discrimination against ^{13}C at the leaf level. This produces non-structural carbohydrates (NSCs) enriched in ^{13}C, which could be used in the

cambium pool during the last months of the growing season (September-October), corresponding with cell wall deposition in the last latewood tracheid (Namvar et al. 2024) Consequently, unreacted ^{13}C-enriched residual sugars such as sucrose (Rinne et al. 2015) may be transported through the phloem and ultimately used for wood formation, mostly for the production of latewood (Namvar et al. 2024), while less enriched NSCs (e.g., pinitol and lipids) are allocated to frost protection in various parts of tree (Rinne et al. 2015; Sleptsov et al. 2023). In this regard, a compound-specific monitoring of carbon stable isotopes in the cambium-xylem continuum (e.g., $\delta^{13}C$ in different sugars found in the two tissues) may offer deeper insights into seasonal carbon allocation strategies in boreal trees. Lastly, it is also possible that the behavior of g_s is driven by shifts in sink demand rather than by external factors such as climatic variations. For example, a reduction in g_s can be driven by a shift from primary to secondary growth during xylogenesis, which would require adjustments in tradeoffs between carbon assimilated and water losses through stomata. To investigate this, linking weekly $\delta^{13}C$-derived intrinsic water use efficiency (iWUE) data with wood anatomy and seasonal xylogenesis dynamics would offer deeper insights into such ecophysiological interactions (Cartenì et al., 2018).

Eastern Canada's black spruces' cambial and developing xylem display contrasting $\delta^{18}O$ trends which suggests that the two tissues may be fed by differing water sources (Barbour et al. 2004). Indeed, this is highlighted by a marked increase in $\delta^{18}O_{cam}$ which contrasts with a decreasing pattern in $\delta^{18}O_{xc}$ (Fig. 3). The $\delta^{18}O_{cam}$ is expected to reflect the $\delta^{18}O$ signals in leaf water transferred to NSCs, the primary photosynthetic products, unloaded from the phloem into the cambial region. By contrast, $\delta^{18}O_{xc}$ signals seem to partially derive from the isotopically depleted upward-moving xylem water from the soil (Roden et al. 2000; Barbour and Farquhar 2000; Barbour et al. 2004; Song et al. 2014b).

Proportional exchanges between the un-enriched xylem water and sugars during the formation of cellulose in the developing xylem (i.e., P_{ex} effect) may explain the depletion of $\delta^{18}O_{xc}$ (Sternberg et al., 1986; Roden et al. 2000; Gessler et al. 2009; Song et al. 2014b). In support of our finding, a study by Offermann et al. (2011) on European beech (*Fagus sylvatica* L.) demonstrated that $\delta^{18}O$ in tree-ring whole wood was not positively related to leaf water evaporative enrichment and $\delta^{18}O$ of NSC pools, highlighting the important role of P_{ex} effect in modifying $\delta^{18}O$ signals in tree ring. Similar findings were reported by Martínez-Sancho et al. (2023), where source water had dominant influence on intra-annual $\delta^{18}O$ variations in tree-ring cellulose of larch (*Larix decidua* L.) in the Swiss Alps, masking signals from needle-level processes. Our results indicate a strong P_{ex} effect, capable of altering the oxygen isotopic signature of cellulose in the xylem cells (Martínez-Sancho et al. 2023). This effect likely represents the largest modification of $\delta^{18}O$ signal between the leaves and tree rings (Siegwolf et al. 2023).

Increasing proportional oxygen isotope exchange between xylem water (source water) and NSCs during the growing season can transform the rising $\delta^{18}O_{cam}$ signal into a decreasing trend in $\delta^{18}O_{xc}$ in black spruce (Fig. 5). This divergence is likely driven by intensified post-photosynthetic exchange (P_{ex}) processes that progressively replace the $^{\delta 18}O$ signature acquired at the leaf level with that of local water during cellulose synthesis (Gessler et al. 2014). Oxygen isotopic composition in tree-ring cellulose reflects both the evaporative enrichment of leaf water and the degree of exchange between sugars and ambient water during transport and metabolism (Roden et al. 2000; Cernusak et al. 2005). When P_{ex} increases, due to higher metabolic turnover, prolonged carbohydrate residence time, or increased cellular hydration in summer, the $\delta^{18}O$ signal from enriched leaf water becomes increasingly overwritten by the more depleted isotopic signature of xylem water (Barbour et al. 2004; Cernusak et al. 2005; Gessler et al. 2009; Gessler et al. 2014). As a result, $\delta^{18}O_{xc}$ can decline, even while $\delta^{18}O_{cam}$ continues to rise due to leaf level physiological processes.

This mechanism has been further supported by recent work from Szejner et al. (2020), who demonstrated that post-photosynthetic fractionation processes, including exchange with water during cellulose biosynthesis, can substantially alter the $\delta^{18}O$ signal inherited from leaf water. Their results across coniferous tree species (*Pinus ponderosa* and *Pseudotsuga menziesii*) and environmental conditions confirmed that intra-seasonal and inter-annual $\delta^{18}O$ patterns in tree-ring cellulose are strongly influenced by P_{ex} dynamics, mostly when increasing during the growing season, which may vary with phenology, water availability, and tissue-specific metabolic activity. In our spruce stands, $\delta^{18}O_{xc\text{-}sim}$ under increasing P_{ex} values (i.e., from 0.3 to 0.5) mirrored these findings, showing decreasing trends that contrasted with the increasing $\delta^{18}O_{cam}$ signal. The effect was particularly evident during late-season wood formation, when extended sugar residence times, likely related to increased sugar concentrations for frost resistance and prevent cellular lysis (Charrier and Améglio 2011), may have enhanced opportunities for exchange. This pattern is consistent with previous studies emphasizing the role of seasonal dynamics in carbohydrate transport and cellulose synthesis (Barbour et al. 2004; Gessler et al. 2009; Offermann et al. 2011).

Previous studies indicated that $\delta^{18}O_{rain}$ varies with temperature, latitude and altitude, showing greater depletion at higher altitudes with lower temperatures (Bortolami et al. 1979; Poage and Chamberlain 2001). The location of BER site, at a higher latitude and altitude with a lower annual mean temperature compared to SIM, likely contributes to the more depleted $\delta^{18}O_{rain}$ signals at this site (Table S10). The $\delta^{18}O$ ratios in different tree compartments are influenced by $\delta^{18}O_{rain}$ signals, leading to lower $\delta^{18}O_{cam}$ and $\delta^{18}O_{xc}$ values in BER compared to SIM (Table S4, mean $\delta^{18}O_{cam}$ and $\delta^{18}O_{xc}$ in SIM were significantly more enriched compared to BER by 1.1 ‰ ($p < 0.01$) for 2020 and 0.7 ‰ for 2021 ($p < 0.01$), not shown in the results section). Additionally, warmer summers in SIM may contribute to an increased soil water evaporation rate, resulting in an increased enrichment in source water, leading to the more enriched $\delta^{18}O_{cam}$ and $\delta^{18}O_{xc}$ values observed at this site compared to BER.

However, the $\delta^{18}O_{xc}$ series do not fully reflect the signature of $\delta^{18}O_{rain}$ during the growing season at our sites (Table 3). This discrepancy may be attributed to two main factors. First, because the exchange of oxygen isotopes between xylem water and NSCs occurs in a proportional manner (i.e., increasing P_{ex}) during the growing season, strong links between weekly $\delta^{18}O_{rain}$ and $\delta^{18}O_{xc}$ signals are not evident. Second, complex environmental processes may alter $\delta^{18}O_{rain}$ signals before it is incorporated into tree tissues. For example, only a portion of total precipitation infiltrates the soil, reaches the roots, and is ultimately absorbed by trees. As water infiltrates the soil, further fractionation can occur, especially during periods of high evaporative demand like summers. Consequently, $\delta^{18}O$ of soil water ($\delta^{18}O_{sw}$) may vary with depth depending on soil structure, season, and climate (Sprenger et al. 2016). Since roots can access water from a range of soil depths, the $\delta^{18}O$ of source water (and of xylem water) may differ from the initial meteoric water inputs (Siegwolf et al. 2023). The discrepancy between weekly $\delta^{18}O_{xc}$ signals and $\delta^{18}O_{rain}$ variations observed here, underscores the need for further investigation into the relationships between weekly $\delta^{18}O_{sw}$ and $\delta^{18}O_{xc}$ signals in spruce stands, potentially shedding light on the hydrodynamics of source water affecting $\delta^{18}O_{xc}$ at seasonal scales (Thomas et al. 2018).

5. Conclusions

Overall, our findings underscore the complexities inherent in using the isotopic signature of xylem cellulose, a common tool in dendroclimatology. This signature results from a multifaceted and cumulative array of processes affecting the end signal. Both carbon and oxygen isotopes in the cambium were influenced by g_s. Xylem carbon isotopes also appeared to derive directly from the leaf and cambial region. This finding is in accordance with previous studies demonstrating strong correlations between isotope composition of new assimilates and tree rings in evergreen coniferous species (Gessler et al. 2009; Rinne--Garmston et al. 2023). In contrast, xylem oxygen isotopes were more

complex and the P_{ex} effect, with increasing trend during the growing season, seemed strong enough to obscure the g_s signal. This complexity cautioned against oversimplistic assumptions that oxygen isotopes in xylem cellulose serve as a reliable proxy for g_s signals, particularly in boreal forests. Our findings highlighted the need for careful consideration of the processes influencing isotopic signals to avoid misinterpretations in dendroclimatological studies.

Moving forward, further research is needed to understand the role of $\delta^{18}O_{sw}$ dynamics in influencing oxygen isotope signals in forming tree rings. Additionally, linking weekly $\delta^{13}C$-derived intrinsic water use efficiency (iWUE) data with wood anatomy and seasonal xylogenesis dynamics may offer deeper insights into interactions among physiological factors, such as sink-driven influences on g_s, in tree species. Expanding this research to other regions, climatic contexts, and species with different growth dynamics and characteristics such as stem diameter (i.e., distance from pith), crown condition, and root depth will enhance our understanding of these processes and improve the robustness of dendroclimatological models across diverse ecosystems. Such interdisciplinary approaches are crucial for understanding how environmental changes may affect tree physiology and xylem hydraulic conductivity over seasonal and decadal scales.

Funding

This work was funded by the National Sciences and Engineering Research Council of Canada (NSERC) to Étienne Boucher (RGPIN 2021-04216).

CRediT authorship contribution statement

Sepideh Namvar: Writing – review & editing, Writing – original draft, Methodology, Formal analysis. **Étienne Boucher:** Writing – review & editing, Supervision, Funding acquisition, Formal analysis. **Annie Deslauriers:** Writing – review & editing. **Fabio Gennaretti:** Writing – review & editing. **Hubert Morin:** Writing – review & editing.

Declaration of competing interest

The authors declare that they have no known competing financial interests or personal relationships that could have appeared to influence the work reported in this paper.

Acknowledgements

We thank François Gionest for his efforts in sample collection and for providing meteorological data. We also thank Caroline Malatrait for designing the sampling sites map using QGIS.

Supplementary materials

Supplementary material associated with this article can be found, in the online version, at doi:10.1016/j.agrformet.2025.110768.

Data availability

The isotope measurements will be available here: https://quebeclabradortr.shinyapps.io/TRdashboard4/. Additional data will be available from a GitHub repository, upon publication of the article.

References

Arora, R., 2018. Mechanism of freeze-thaw injury and recovery: *a cool retrospective and warming up to new ideas*. Plant Sci. 270, 301–313.
Baldocchi, D.D., 2020. How eddy covariance flux measurements have contributed to our understanding of Global Change Biology. Glob. Change Biol. 26, 242–260.
Balducci, L., Deslauriers, A., De Barba, D., Rossi, S., Houle, D., Bergeron, Y., Morin, H., 2021. Influence of soil warming and N-addition on sap flux density and stem radius variation in boreal stands in Quebec, Canada. Ecohydrology 14, e2261.
Ballantyne, A.P., Miller, J.B., Tans, P.P., 2010. Apparent seasonal cycle in isotopic discrimination of carbon in the atmosphere and biosphere due to vapor pressure deficit. Glob. Biogeochem. Cycles. 24, 2009GB003623.
Barbour, M.M., Farquhar, G.D., 2000. Relative humidity- and ABA-induced variation in carbon and oxygen isotope ratios of cotton leaves. Plant Cell Environ. 23, 473–485.
Barbour, M.M., Roden, J.S., Farquhar, G.D., Ehleringer, J.R., 2004. Expressing leaf water and cellulose oxygen isotope ratios as enrichment above source water reveals evidence of a Péclet effect. Oecologia 138, 426–435.
Barbour, M.M., Schurr, U., Henry, B.K., Wong, S.C., Farquhar, G.D., 2000. Variation in the oxygen isotope ratio of Phloem Sap sucrose from Castor Bean. Evidence in support of the péclet effect. Plant. Physiol. 123, 671–680.
Barbour, M.M., Walcroft, A.S., Farquhar, G.D., 2002. Seasonal variation in δ13C and δ18O of cellulose from growth rings of Pinus radiata. Plant. Cell Environ. 25, 1483–1499.
Beer, C., Reichstein, M., Tomelleri, E., Ciais, P., Jung, M., Carvalhais, N., Rödenbeck, C., Arain, M.A., Baldocchi, D., Bonan, G.B., Bondeau, A., Cescatti, A., Lasslop, G., Lindroth, A., Lomas, M., Luyssaert, S., Margolis, H., Oleson, K.W., Roupsard, O., Veenendaal, E., Viovy, N., Williams, C., Woodward, F.I., Papale, D., 2010. Terrestrial gross carbon dioxide uptake: global distribution and covariation with climate. Science 329, 834–838.
Bégin, C., Gingras, M., Savard, M.M., Marion, J., Nicault, A., Bégin, Y., 2015. Assessing tree-ring carbon and oxygen stable isotopes for climate reconstruction in the Canadian northeastern boreal forest. Palaeogeogr. Palaeoclimatol. Palaeoecol. 423, 91–101.
Belmecheri, S., Lavergne, A., 2020. Compiled records of atmospheric CO2 concentrations and stable carbon isotopes to reconstruct climate and derive plant ecophysiological indices from tree rings. Dendrochronologia 63, 125748.
Belmecheri, S., Wright, W.E., Szejner, P., Morino, K.A., Monson, R.K., 2018. Carbon and oxygen isotope fractionations in tree rings reveal interactions between cambial phenology and seasonal climate. Plant. Cell Environ. 41, 2758–2772.
Bortolami G.C., Ricci B., Susella G.F. (1979) Isotope hydrology of the Val Corsaglia Maritime alps, Piedmont, Italy.
Bozonnet, C., Saudreau, M., Badel, E., Améglio, T., Charrier, G., 2024. Freeze dehydration vs supercooling in tree stems: physical and physiological modelling. Tree Physiol. 44, tpad117.
Buckley, T.N., 2017. Modeling stomatal conductance. Plant Physiol 174, 572–582.
Burke, M.J., Gusta, L.V., Quamme, H.A., Weiser, C.J., Li, P.H., 1976. Freezing and injury in plants. Annu. Rev. Plant Biol. 27, 507–528.
Buttò, V., Rossi, S., Deslauriers, A., Morin, H., 2019. Is size an issue of time? Relationship between the duration of xylem development and cell traits. Ann. Bot 123, 1257–1265.
Cartenì, F., Deslauriers, A., Rossi, S., Morin, H., De Micco, V., Mazzoleni, S., Giannino, F., 2018. The physiological mechanisms behind the earlywood-to-latewood transition: a process-based modeling approach. Frontiers in Plant Science 9, 1053.
Castagneri, D., Battipaglia, G., Von Arx, G., Pacheco, A., Carrer, M., 2018. Tree-ring anatomy and carbon isotope ratio show both direct and legacy effects of climate on bimodal xylem formation in Pinus pinea Cernusak L (ed). Tree Physiol. 38, 1098–1109.
Cernusak, L.A., Farquhar, G.D., Pate, J.S., 2005. Environmental and physiological controls over oxygen and carbon isotope composition of Tasmanian blue gum, eucalyptus globulus. Tree Physiol. 25, 129–146.
Charrier, G., Améglio, T., 2011. The timing of leaf fall affects cold acclimation by interactions with air temperature through water and carbohydrate contents. Environ. Exp. Bot 72, 351–357.
Charrier, G., Améglio, T., 2024. Dynamic modeling of stem water content during the dormant period in walnut trees. Tree Physiol. 44, tpad128.
Charrier, G., Cochard, H., Améglio, T., 2013. Evaluation of the impact of frost resistances on potential altitudinal limit of trees. Tree Physiol. 33, 891–902.
Danis, P.A., Masson-Delmotte, V., Stievenard, M., Guillemin, M.T., Daux, V., Naveau, Ph, Von Grafenstein, U., 2006. Reconstruction of past precipitation δ18O using tree-ring cellulose δ18O and δ13C: a calibration study near Lac d'Annecy, France. Earth Planet Sci. Lett. 243, 439–448.
Dao, M.C.E., Rossi, S., Walsh, D., Morin, H., Houle, D., 2015. A 6-year-long manipulation with soil warming and canopy nitrogen additions does not affect xylem phenology and cell production of mature black spruce. Front Plant Sci. 6. http://journal.frontiersin.org/Article/10.3389/fpls.2015.00877/abstract, 5 September 2024, date last accessed.
Deslauriers, A., Giovannelli, A., Rossi, S., Castro, G., Fragnelli, G., Traversi, L., 2009. Intra-annual cambial activity and carbon availability in stem of poplar. Tree Physiol. 29, 1223–1235.
Deslauriers, A., Huang, J.-G., Balducci, L., Beaulieu, M., Rossi, S., 2016. The contribution of carbon and water in modulating wood formation in black spruce saplings. Plant Physiol. 170, 2072–2084.
Epstein, S., Yapp, C.J., Hall, J.H., 1976. The determination of the D/H ratio of non-exchangeable hydrogen in cellulose extracted from aquatic and land plants. Earth Planet Sci. Lett. 30, 241–251.
Farquhar, G.D., Barbour, M.M., Henry, B.K., 1998. Interpretation of oxygen isotope composition of leaf material. Stable Isotopes. Garland Science.
Farquhar, G.D., Lloyd, J., 1993. 5 - Carbon and oxygen isotope effects in the exchange of Carbon dioxide between terrestrial plants and the atmosphere. In: Ehleringer, J.R., Hall, A.E., Farquhar, G.D. (Eds.), Stable Isotopes and Plant Carbon-Water Relations. Academic Press, San Diego, pp. 47–70. https://www.sciencedirect.com/science/article/pii/B9780080918013500118, 17 June 2024, date last accessed.

Farquhar, G.D., Sharkey, T.D., 1982. Stomatal conductance and photosynthesis. Annu. Rev. Plant Physiol. 33, 317–345.
Flexas, J., Diaz-Espejo, A., Gago, J., Gallé, A., Galmés, J., Gulías, J., Medrano, H., 2013. Photosynthetic limitations in Mediterranean plants: a review. Environ. Exp. Bot. 103, 12–23.
Fonti, M., Vaganov, E., Wirth, C., Shashkin, A., Astrakhantseva, N., Schulze, E.-D., 2018. Age-effect on intra-annual δ13C-variability within Scots pine tree-rings from Central Siberia. Forests 9, 364.
Fu, P.-L., Grießinger, J., Gebrekirstos, A., Fan, Z.-X., Bräuning, A., 2017. Earlywood and latewood stable carbon and oxygen isotope variations in two pine species in southwestern China during the recent decades. Front Plant. Sci. 7. http://journal.frontiersin.org/article/10.3389/fpls.2016.02050/full, 24 July 2023, date last accessed.
Gessler, A., Brandes, E., Buchmann, N., Helle, G., Rennenberg, H., Barnard, R.L., 2009. Tracing carbon and oxygen isotope signals from newly assimilated sugars in the leaves to the tree-ring archive. Plant Cell Environ. 32, 780–795.
Gessler, A., Brandes, E., Keitel, C., Boda, S., Kayler, Z.E., Granier, A., Barbour, M., Farquhar, G.D., Treydte, K., 2013. The oxygen isotope enrichment of leaf-exported assimilates – does it always reflect lamina leaf water enrichment? New Phytol. 200, 144–157.
Gessler, A., Ferrio, J.P., Hommel, R., Treydte, K., Werner, R.A., Monson, R.K., 2014. Stable isotopes in tree rings: towards a mechanistic understanding of isotope fractionation and mixing processes from the leaves to the wood. Tree Physiol. 34, 796–818.
Giovannelli, A., Emiliani, G., Traversi, M.L., Deslauriers, A., Rossi, S., 2011. Sampling cambial region and mature xylem for non structural carbohydrates and starch analyses. Dendrochronologia 29, 177–182.
Grams, T.E.E., Kozovits, A.R., Häberle, K.-H., Matyssek, R., Dawson, T.E., 2007. Combining ? ^{13}C and ? ^{18} O analyses to unravel competition, CO $_2$ and O $_3$ effects on the physiological performance of different-aged trees. Plant Cell Environ. 30, 1023–1034.
Hélie, J., Hillaire-Marcel, C., 2021. Designing working standards for stable H, C, and O isotope measurements in CO $_2$ and H $_2$ O. Rapid. Commun. Mass Spectrom. 35, e9008.
Hilasvuori, E., Berninger, F., Sonninen, E., Tuomenvirta, H., Jungner, H., 2009. Stability of climate signal in carbon and oxygen isotope records and ring width from Scots pine (Pinus sylvestris L.) in Finland. J. Quat. Sci. 24, 469–480.
Hill, S.A., Waterhouse, J.S., Field, E.M., Switsur, V.R., Ap Rees, T., 1995. Rapid recycling of triose phosphates in oak stem tissue. Plant Cell Environ. 18, 931–936.
Keitel, C., Adams, M.A., Holst, T., Matzarakis, A., Mayer, H., Rennenberg, H., GEßLER, A., 2003. Carbon and oxygen isotope composition of organic compounds in the phloem sap provides a short-term measure for stomatal conductance of European beech (*Fagus sylvatica* L.). Plant Cell Environ. 26, 1157–1168.
Klein, T., Hemming, D., Lin, T., Grünzweig, J.M., Maseyk, K., Rotenberg, E., Yakir, D., 2005. Association between tree-ring and needle δ13C and leaf gas exchange in Pinus halepensis under semi-arid conditions. Oecologia 144, 45–54.
Loader, N.J., McCarroll, D., Barker, S., Jalkanen, R., Grudd, H., 2017. Inter-annual carbon isotope analysis of tree-rings by laser ablation. Chem. Geol. 466, 323–326.
Luo, Y.-H., Sternberg, L.D.S.L., 1992. Hydrogen and oxygen isotopic fractionation during heterotrophic cellulose synthesis. J. Exp. Bot. 43, 47–50.
Martínez-Sancho, E., Cernusak, L.A., Fonti, P., Gregori, A., Ullrich, B., Pannatier, E.G., Gessler, A., Lehmann, M.M., Saurer, M., Treydte, K., 2023. Unenriched xylem water contribution during cellulose synthesis influenced by atmospheric demand governs the intra-annual tree-ring δ18O signature. New Phytol. 240, 1743–1757.
McCarroll, D., Loader, N.J., 2004. Stable isotopes in tree rings. Quat Sci. Rev. 23, 771–801.
Namvar, S., Boucher, É., Deslauriers, A., Morin, H., Savard, M.M., 2024. Monitoring weekly δ 13C variations along the cambium-xylem continuum in the Canadian eastern boreal forest. Tree Physiol tpae136.
Naulier, M., Savard, M.M., Bégin, C., Marion, J., Arseneault, D., Bégin, Y., 2014. Carbon and oxygen isotopes of lakeshore black spruce trees in northeastern Canada as proxies for climatic reconstruction. Chem Geol. 374–375, 37–43.
Offermann, C., Ferrio, J.P., Holst, J., Grote, R., Siegwolf, R., Kayler, Z., Gessler, A., 2011. The long way down—are carbon and oxygen isotope signals in the tree ring uncoupled from canopy physiological processes? Tree Physiol. 31, 1088–1102.
Ogée, J., Barbour, M.M., Wingate, L., Bert, D., Bosc, A., Stievenard, M., Lambrot, C., Pierre, M., Bariac, T., Loustau, D., Dewar, R.C., 2009. A single-substrate model to interpret intra-annual stable isotope signals in tree-ring cellulose. Plant Cell Environ. 32, 1071–1090.
Poage, M.A., Chamberlain, C.P., 2001. Empirical relationships between elevation and the stable isotope composition of precipitation and surface waters: considerations for studies of paleoelevation change. Am. J. Sci. 301, 1–15.
Pons, T.L., Helle, G., 2011. Identification of anatomically non-distinct annual rings in tropical trees using stable isotopes. Trees 25, 83–93.
Raffalli-Delerce, G., Masson-Delmotte, V., Dupouey, J.L., Stievenard, M., Breda, N., Moisselin, J.M., 2004. Reconstruction of summer droughts using tree-ring cellulose isotopes: a calibration study with living oaks from Brittany (western France). Tellus B 56, 160–174.
Rinne, K.T., Saurer, M., Kirdyanov, A.V., Loader, N.J., Bryukhanova, M.V., Werner, R.A., Siegwolf, R.T.W., 2015. The relationship between needle sugar carbon isotope ratios and tree rings of larch in Siberia Cernusak L (ed). Tree Physiol. tpv096.
Rinne-Garmston, K.T., Tang, Y., Sahlstedt, E., Adamczyk, B., Saurer, M., Salmon, Y., Carrasco, M., del, R.D., Hölttä, T., Lehmann, M.M., Mo, L., Young, G.H.F., 2023. Drivers of intra-seasonal δ13C signal in tree-rings of Pinus sylvestris as indicated by compound-specific and laser ablation isotope analysis. Plant Cell Environ. 46, 2649–2666.
Roden, J.S., Ehleringer, J.R., 1999. Hydrogen and oxygen isotope ratios of tree-ring cellulose for riparian trees grown long-term under hydroponically controlled environments. Oecologia 121, 467–477.
Roden, J.S., Lin, G., Ehleringer, J.R., 2000. A mechanistic model for interpretation of hydrogen and oxygen isotope ratios in tree-ring cellulose. Geochim Cosmochim. Acta. 64, 21–35.
Rossi, S., Morin, H., Deslauriers, A., Plourde, P.-Y., 2011. Predicting xylem phenology in black spruce under climate warming. Glob. Change Biol. 17, 614–625.
Sarris, D., Siegwolf, R., Körner, C., 2013. Inter- and intra-annual stable carbon and oxygen isotope signals in response to drought in Mediterranean pines. Agric. For Meteorol. 168, 59–68.
Sass-Klaassen, U., Poole, I., Wils, T., Helle, G., Schleser, G.H., van Bergen, P.F., 2005. Carbon and oxygen isotope dendrochronology in sub-fossil bog oak tree rings - A preliminary study. IAWA J. 26, 121–136.
Saurer, M., Sahlstedt, E., Rinne-Garmston, K.T., Lehmann, M.M., Oettli, M., Gessler, A., Treydte, K., 2023. Progress in high-resolution isotope-ratio analysis of tree rings using laser ablation Epron D (ed). Tree Physiol. 43, 694–705.
Scheidegger, Y., Saurer, M., Bahn, M., Siegwolf, R., 2000. Linking stable oxygen and carbon isotopes with stomatal conductance and photosynthetic capacity: a conceptual model. Oecologia 125, 350–357.
Schiestl-Aalto, P., Ryhti, K., Mäkelä, A., Peltoniemi, M., Bäck, J., Kulmala, L., 2019. Analysis of the NSC storage dynamics in tree organs reveals the allocation to belowground symbionts in the framework of whole tree carbon balance. Front For Glob. Change 2, 17.
Schollaen, K., Heinrich, I., Helle, G., 2014. UV -laser-based microscopic dissection of tree rings – a novel sampling tool for δ ^{13}C and δ ^{18} O studies. New Phytol. 201, 1045–1055.
Siegwolf, R.T.W., Lehmann, M.M., Goldsmith, G.R., Churakova (Sidorova), O.V., Mirande-Ney, C., Timoveeva, G., Weigt, R.B., Saurer, M., 2023. Updating the dual C and O isotope—gas-exchange model: a concept to understand plant responses to the environment and its implications for tree rings. Plant Cell Environ. 46, 2606–2627.
Siegwolf, R.T.W., Lehmann, M., Goldsmith, G., Churakova, O., Mirande-Ney, C., Gruspante, G., Weigt, R., Saurer, M., 2021. The dual C and O isotope – gas exchange model: a concept review for understanding plant responses to the environment and its application in tree rings. Authorea Preprints.
Simard, S., Giovannelli, A., Treydte, K., Traversi, M.L., King, G.M., Frank, D., Fonti, P., 2013. Intra-annual dynamics of non-structural carbohydrates in the cambium of mature conifer trees reflects radial growth demands. Tree Physiol. 33, 913–923.
Sleptsov, I.V., Mikhailov, V.V., Rozhina, S.M., Kershengolts, B.M., 2023. The year-round dynamic of metabolites accumulation in Pinus sylvestris needles in permafrost zone. Trees 37, 285–296.
Song, X., Clark, K.S., Helliker, B.R., 2014a. Interpreting species-specific variation in tree-ring oxygen isotope ratios among three temperate forest trees. Plant Cell Environ. 37, 2169–2182.
Song, X., Farquhar, G.D., Gessler, A., Barbour, M.M., 2014b. Turnover time of the non-structural carbohydrate pool influences δ^{18} O of leaf cellulose. Plant Cell Environ. 37, 2500–2507.
Soudant, A., Loader, N.J., Bäck, J., Levula, J., Kljun, N., 2019. Intra-annual variability of wood formation and δ13C in tree-rings at Hyytiälä, Finland. Agricultural and Forest Meteorology 224, 17–29.
Sprenger, M., Leistert, H., Gimbel, K., Weiler, M., 2016. Illuminating hydrological processes at the soil-vegetation-atmosphere interface with water stable isotopes. Rev. Geophys. 54, 674–704.
Sternberg, L.D.S.L.O., 2009. Oxygen stable isotope ratios of tree-ring cellulose: the next phase of understanding. New Phytol. 181, 553–562.
Sternberg, L.D.S., Deniro, M.J., Savidge, R.A., 1986. Oxygen isotope exchange between metabolites and water during biochemical reactions leading to cellulose synthesis. Plant physiology 82 (2), 423–427.
Szejner, P., Clute, T., Anderson, E., Evans, M.N., Hu, J., 2020. Reduction in lumen area is associated with the δ ^{18} O exchange between sugars and source water during cellulose synthesis. New Phytol. 226, 1583–1593.
Szymczak S., Joachimski M.M., Bräuning A., Hetzer T., Kuhlemann J. (2012) A 560 yr summer temperature reconstruction for the Western Mediterranean basin based on stable carbon isotopes from <i>Pinus nigra</i> ssp. <i>laricio</i> (Corsica/France). https://cp.copernicus.org/preprints/8/2111/2012/cpd-8-2111-2012.pdf (11 October 2024, date last accessed).
Thomas, F.M., Rzepecki, A., Lücke, A., Wiekenkamp, I., Rabbel, I., Pütz, T., Neuwirth, B., 2018. Growth and wood isotopic signature of Norway spruce (*Picea abies*) along a small-scale gradient of soil moisture Cernusak L (ed). Tree Physiol. 38, 1855–1870.
Treydte, K., Boda, S., Graf Pannatier, E., Fonti, P., Frank, D., Ullrich, B., Saurer, M., Siegwolf, R., Battipaglia, G., Werner, W., Gessler, A., 2014. Seasonal transfer of oxygen isotopes from precipitation and soil to the tree ring: source water versus needle water enrichment. New Phytol. 202, 772–783.
Turcotte, A., Morin, H., Krause, C., Deslauriers, A., Thibeault-Martel, M., 2009. The timing of spring rehydration and its relation with the onset of wood formation in black spruce. Agric. Meteorol. 149, 1403–1409.
Turcotte, A., Rossi, S., Deslauriers, A., Krause, C., Morin, H., 2011. Dynamics of depletion and replenishment of water storage in stem and roots of black spruce measured by dendrometers. Front Plant. Sci. 2. http://journal.frontiersin.org/article/10.3389/fpls.2011.00021/abstract, 27 September 2024, date last accessed.

Waterhouse, J.S., Switsur, V.R., Barker, A.C., Carter, A.H.C., Robertson, I., 2002. Oxygen and hydrogen isotope ratios in tree rings: how well do models predict observed values? Earth Planet Sci. Lett. 201, 421–430.
Xu, G., Liu, X., Hu, J., Dorado-Liñán, I., Gagen, M., Szejner, P., Chen, T., Trouet, V., 2022. Intra-annual tree-ring δ18O and δ13C reveal a trade-off between isotopic source and humidity in moist environments Cernusak L (ed). Tree Physiol. tpac076.
Young, G.H.F., Demmler, J.C., Gunnarson, B.E., Kirchhefer, A.J., Loader, N.J., McCarroll, D., 2011. Age trends in tree ring growth and isotopic archives: a case study of Pinus sylvestris L. from northwestern Norway. Glob. Biogeochem. Cycles 25. https://Nlibrary.wiley.com/doi/abs/10.1029/2010GB003913, 11 October 2024, date last accessed.